Received: 10 October 2023 | Revised: 22 November 2023 | Accepted: 24 November 2023

DOI: 10.1002/ardp.202300583

ARCH PHARM DPhG
Archiv der Pharmazie

FULL PAPER

A combined approach of structure-based virtual screening and NMR to interrupt the PD-1/PD-L1 axis: Biphenyl-benzimidazole containing compounds as novel PD-L1 inhibitors

Greta Donati[1] | Monica Viviano[2] | Vincenzo Maria D'Amore[1] | Alessandra Cipriano[2] | Isidora Diakogiannaki[1] | Jussara Amato[1] | Stefano Tomassi[1] | Diego Brancaccio[1] | Pasquale Russomanno[1] | Francesco Saverio Di Leva[1] | Daniela Arosio[3] | Pierfausto Seneci[4] | Sabrina Taliani[5] | Katarzyna Magiera-Mularz[6] | Bogdan Musielak[6] | Lukasz Skalniak[6] | Tad A. Holak[6] | Sabrina Castellano[2] | Valeria La Pietra[1] | Luciana Marinelli[1]

[1]Department of Pharmacy, University of Naples Federico II, Naples, Italy

[2]Department of Pharmacy, University of Salerno, Fisciano, Italy

[3]Istituto di Scienze e Tecnologie Chimiche "Giulio Natta" (SCITEC), Consiglio Nazionale delle Ricerche (CNR), Milan, Italy

[4]Department of Chemistry, University of Milan, Milan, Italy

[5]Department of Pharmacy, University of Pisa, Pisa, Italy

[6]Department of Organic Chemistry, Faculty of Chemistry, Jagiellonian University, Cracow, Poland

Correspondence
Luciana Marinelli and Valeria La Pietra, Department of Pharmacy, University of Naples Federico II, via D. Montesano 49, 80131, Napoli (NA), Italy.
Email: lmarinel@unina.it and valeria.lapietra@unina.it

Sabrina Castellano, Department of Pharmacy, University of Salerno, via Giovanni Paolo II 132, I-84084 Fisciano (SA), Italy.
Email: scastellano@unisa.it

Funding information
Fundacja na rzecz Nauki Polskiej; European Regional Development Fund; Ministero dell'Istruzione, dell'Università e della Ricerca; Italian Ministry of Education, University, and Research (MIUR); Progetti di Rilevante Interesse Nazionale, PRIN 2017, Grant/Award Number: 2017PHRC8X; PRIN

Abstract

Immunotherapy has emerged as a game-changing approach for cancer treatment. Although monoclonal antibodies (mAbs) targeting the programmed cell death protein 1/programmed cell death protein 1 ligand 1 (PD-1/PD-L1) axis have entered the market revolutionizing the treatment landscape of many cancer types, small molecules, although presenting several advantages including the possibility of oral administration and/or reduced costs, struggled to enter in clinical trials, suffering of water insolubility and/or inadequate potency compared with mAbs. Thus, the search for novel scaffolds for both the design of effective small molecules and possible synergistic strategies is an ongoing field of interest. In an attempt to find novel chemotypes, a virtual screening approach was employed, resulting in the identification of new chemical entities with a certain binding capability, the most versatile of which was the benzimidazole-containing compound **10**. Through rational design, a small

Greta Donati, Monica Viviano, and Vincenzo Maria D'Amore contributed equally to this study.

2022, Grant/Award Number: 2022YWZWB2; POIR, Grant/Award Number: 04.04.00-00-420 F/17-00; European Union

library of its derivatives was synthesized and evaluated. The homogeneous time-resolved fluorescence (HTRF) assay revealed that compound **17** shows the most potent inhibitory activity (IC_{50}) in the submicromolar range and notably, differently from the major part of PD-L1 inhibitors, exhibits satisfactory water solubility properties. These findings highlight the potential of benzimidazole-based compounds as novel promising candidates for PD-L1 inhibition.

KEYWORDS

benzimidazole, immunotherapy, NMR, PD-L1 inhibitors, virtual screening

1 | INTRODUCTION

Cancer-targeted therapy is booming, and novel drugs are constantly emerging. Among the most interesting anticancer approacheses-merged so far is immunotherapy. It started with ipilimumab, an anti-CTLA-4 (cytotoxic T-lymphocyte protein 4) monoclonal antibody (mAb), approved in 2011 for the treatment of melanoma, and able to reactivate the immune system against cancer cells.[1] CTLA-4 together with programmed cell death protein 1/programmed cell death protein 1 ligand 1 (PD-1/PD-L1), indoleamine 2,3-dioxygenase (IDO), T-cell immunoglobulin and mucin domain-containing protein 3 (TIM-3), and lymphocyte-activation gene 3 (LAG-3) are the immune checkpoints receptor that have garnered the most attention so far. Specifically, PD-1 binds two natural ligands: PD-L1 and PD-L2 which are both transmembrane proteins belonging to the immunoglobulin superfamily. In cancer cells, overexpression of PD-L1 leads to the progression of T cells into an exhausted state and decreased tumor cell apoptosis. Consequently, blocking PD-1/PD-L1 interaction can restore the function of the immune system in a number of cancer types such as melanoma, breast, pancreatic, renal, and non-small-cell lung (NSCLC) carcinomas, similar to CTLA-4 blockade.[2–6] Currently, all clinically approved anti-PD-1/PD-L1 therapeutics are highly selective mAbs, such as nivolumab, pembrolizumab, cemiplimab, and dostarlimab targeting PD-1, or atezolizumab, avelumab, and durvalumab against PD-L1.[7,8] Once they entered the market, those mAbs have revolutionized the treatment landscape of many cancer types, especially in the metastatic setting. To date, more than 1000 clinical trials have evaluated the antitumor property of anti-PD-1/anti-PD-L1 antibodies, and the list of approvals is constantly expanding toward more and more cancer types. However, to reduce the costs and the side effects of mAbs, while improving the patient's compliance (e.g., oral administration), the finding and developing of small molecules as PD-1/PD-L1 inhibitors has started. In fact, low-molecular-weight ligands are less expensive and have even the advantages of higher tissue permeability, and more controllable pharmacokinetics, providing, at least in principle, a promising alternative strategy to mAbs. In recent years, an extensive work on biphenyl-containing molecules -like the compound Bristol Myers Squibb (BMS)-202 (**1**) -[9] has firstly resulted in an impressive number of patents and later in publications and led to important advances in the field of PD-1/PD-L1 small molecule inhibitors (see Figure 1).[10-14] Among all, the most promising results have been shown in 2021 for ARB-272572,[15] a C2-symmetrical structure with significative activity on mice and with evixapodlin,[16] MAX-10181[17] and INCB086550,[18] being the most advanced one (clinical phase II).

Nonetheless, they still lack the level of in vivo activity displayed by mAbs and most of them suffer from insolubility problems and/or toxicological issues, so the research of more soluble small molecules and possible synergistic strategies must go on. Interestingly, a new wave of anti-PD-L1-based therapies encompasses a combination of mAbs and anti-PD-L1 small molecules.[19] Herein, in the attempt to find novel chemotypes, with potentially improved water solubility (a known limit of most PD-L1 inhibitors), a virtual screening (VS) of the ZINC12 database (DB) and of an in-house DB[20] has been performed and the most promising virtually-identified hits (11 compounds) were screened by performing one-dimensional (1D) nucleic magnetic resonance (NMR) experiments with PD-L1 protein. As a result, five molecules displayed a certain binding capability to PD-L1. Among these, we selectively focused on EML258 (10), due to our knowledge in benzimidazole medicinal chemistry[21-23] and to its property as a privileged scaffold. In fact, this hetero-aromatic bicyclic ring is metabolically stable, synthetically accessible, and offers a high degree of structural diversity. Several literature reports indicate that diversely substituted benzimidazoles feature distinct pharmacological activity and have found applications in diverse therapeutic areas, such as cancer, inflammatory disorders, viral, bacterial, and parasitic infections.[24-28] Thus, starting from **10** we synthesized a small library of derivatives. Among the novel compounds, the homogeneous time-resolved fluorescence (HTRF) binding assay revealed that compound **17** is the most potent one in interrupting the PD-1/PD-L1 complex (IC_{50} in the submicromolar range). Notably, differently from the major part of PD-L1 inhibitors, it exhibits unexpected satisfactory solubility properties. Through two-dimensional (2D) NMR, we unambiguously identified the binding site where **17** is hosted, which turned out to be almost superimposable to that of **1**. A combined approach of NMR and molecular docking calculations revealed the interaction mode within PD-L1 paving the way for further optimization in binding affinities. Altogether, these findings highlight the potential of our new benzimidazole-based compounds as novel, promising candidates for effective PD-L1 inhibition.

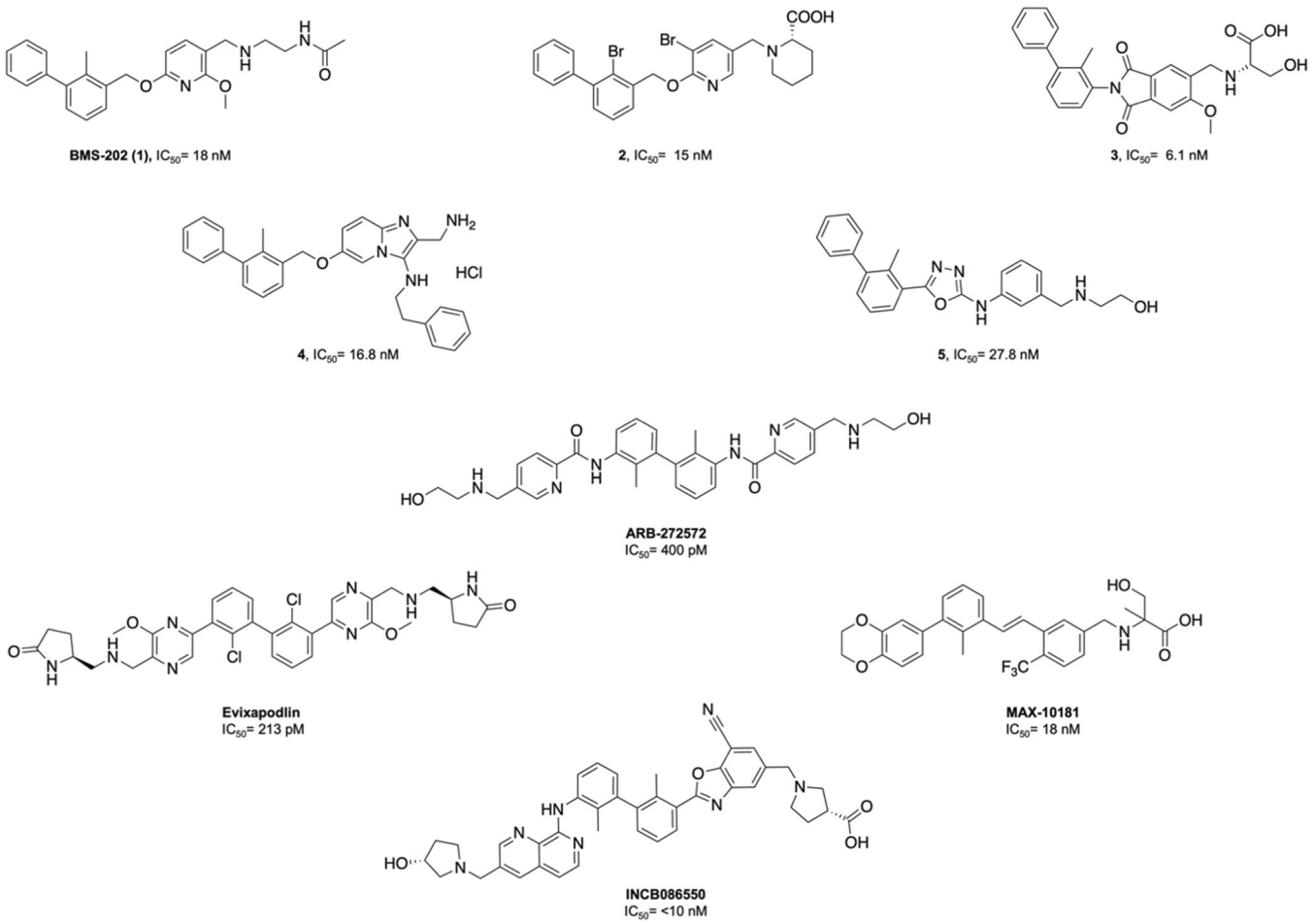

FIGURE 1 Chemical structures of the most representative programmed cell death protein 1 ligand 1 (PD-L1) inhibitors along with their IC_{50} values.

2 | RESULTS AND DISCUSSION

2.1 | Virtual screening

The analysis of anti-PD-L1 biphenyl-containing ligands has inspired the development of several pharmacophore models.[12,29-32] Despite small differences in accessory points, all models present a central aromatic scaffold, a biphenyl moiety, and a basic amine group (see Supporting Information S1: Figure S1). The relative distances between the aromatic moieties, in the known ligands, can be slightly different. Generally, most of the active compounds known so far possess a two-atoms linker between the biphenyl and the central scaffold (as in compounds **1**, **2**, **4**),[9,10,12,14] which can be even part of a cycle (see compound **3** in Figure 1),[11] less frequently, a bit longer linker is present (see compound **5** in Figure 1).[13] Lately, we published a five-points pharmacophore model for extended/symmetrical biphenyl ligands.[29] As the aim of the present study was to find novel small PD-L1 binders, we used a simplified version of our model, containing three aromatic points (one for the central scaffold and two for the biphenyl moiety) and a positively charged point to mimic the basic amine function (Supporting Information S1: Figure S1). The subset "Leads Now" of the ZINC12 DB (about 2 million compounds) together with an in-house library of ~4000 small molecules[20] was screened with the aid of such a pharmacophoric model. Only those structures matching all the four points were retained for subsequent docking-based VS. Thus, almost 900 hits were docked into the dimeric structure of PD-L1 (PDB code: 5J89)[30] by means of Glide.[33] The receptor-based screening returned ~180 hits that were all visually inspected. The final choice was made based on the superposition with **1**, on their chemical heterogeneity, and on the synthetic feasibility. Thus, 11 hits (**6**–**16**), seven from our in-house DB (LOR1, 11752305, CDM-55, EML432, EML258, EML746, 1332287), and four from the ZINC DB (Z1686815855, Z295636908, Z109836016, Z110038292; name or ZINC codes and chemical structure visible in Table 1) were selected for NMR 1D screening.

2.2 | NMR binding assay

The binding capabilities of the selected compounds (**11**) were evaluated by ^{1}H NMR spectroscopy. Small molecule inhibitors were

TABLE 1 Names or ZINC codes and chemical structures of the 11 compounds selected for NMR evaluation.

Code/name	Chemical structure	Glide score
LOR1 (**6**)	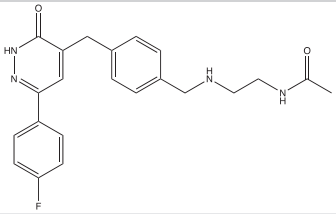	−7.337
11752305 (**7**)	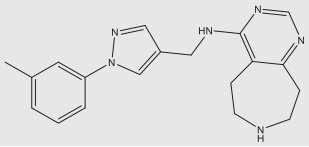	−9.211
CDM-55 (**8**)	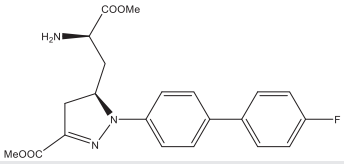	−7.968
EML432 (**9**)	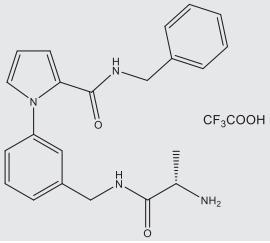	−9.636
EML258 (**10**)	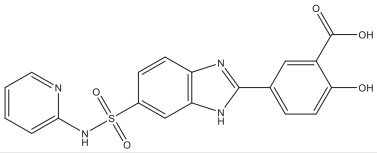	−8.94
EML746 (**11**)	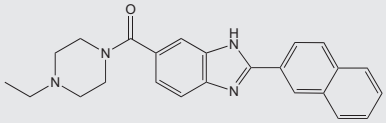	−7.826
Z1686815855 (**12**)	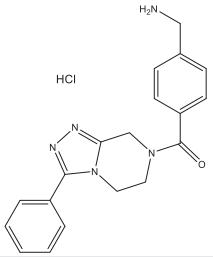	−10.145
Z295636908 (**13**)	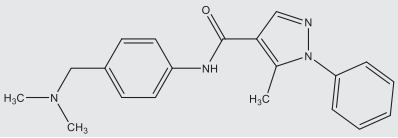	−9.429
Z109836016 (**14**)	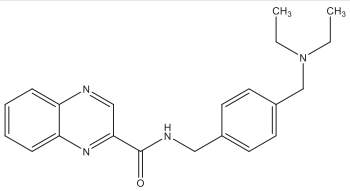	−8.329

TABLE 1 (Continued)

Code/name	Chemical structure	Glide score
Z110038292 (**15**)	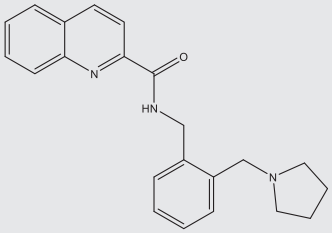	−4.455
1332287 (**16**)	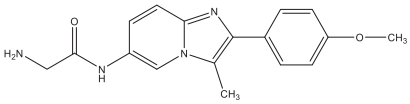	−7.033

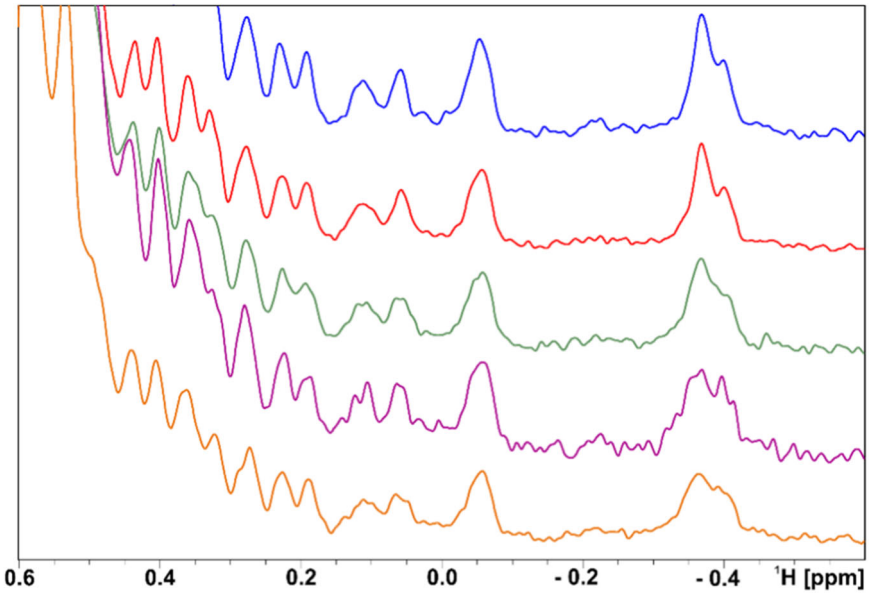

FIGURE 2 Aliphatic part of ^{1}H NMR spectra for the titration of hPD-L1 with 10. Blue: the reference programmed cell death protein 1 ligand 1 (PD-L1); red: PD-L1/10 in the molar ratio 1:1, green: 1:5, purple: 1:10, and orange: only with DMSO, respectively.

tested against PD-1 binding single domain of PD-L1 (amino acids 18–134). We showed that only five of the compounds (**7**, **9**, **10**, **13**, and **14**) bind to PD-L1 at the elevated concentration (molar ratio above 1:5 protein:inhibitor), as the NMR signals splitting were observed (Figure 2; Supporting Information S1: Figure S2). To be sure that in the NMR spectra weak interactions of the inhibitor with the PD-L1 protein were observed, a blank test was also performed using only dimethylsulfoxide (DMSO, in the equivalent volume as the sample used for NMR titration). The results clearly confirmed that the observed changes were due to interactions between the chemical probe and the protein. As the concentration of inhibitor in the sample increases, signals splitting are observed at −0.05 and −0.35 ppm, indicating protein–inhibitor interactions. Despite the aromatic groups in the compound, no broadening of the NMR signals is observed in the spectra as in the case of BMS-like compounds.[34] This indicates that the protein does not undergo oligomerization under the influence of the tested compounds. The behavior of these inhibitors was similar to compound STD4, a weak binder that did not induce oligomerization of PD-L1.[35]

2.3 | Hit optimization

In NMR studies, 5 out of 11 hits were demonstrated to weakly bind PD-L1. Among them, we decided to focus on the benzimidazole-containing compound **10**. In fact, we envisaged that the benzimidazole, a privileged chemotype in medicinal chemistry, metabolically stable and synthetically easily accessible, on which we have synthetic expertise,[22,23] could work as the central aromatic scaffold. Thus, the binding mode of **10** and its superimposition with the crystallographic structure of **1** complexed with dimeric PD-L1, guided hit optimization (Figure 3).

As shown in Figure 3, **10** adapts itself at the hydrophobic surface with the benzene ring of the benzimidazole moiety well superimposed with the central pyridine ring of **1**. Notably, the carboxyl moiety of **10** overlaps with the terminal phenyl ring of **1**, thus residing in the hydrophobic region formed by $_{A}$Met115, $_{A}$Ala121, $_{B}$Ala121, and $_{B}$Tyr123, and undoubtfully represents the first point of modification in the process of hit optimization. On the other side of the molecule, the basic pyridine ring is too far away to form a

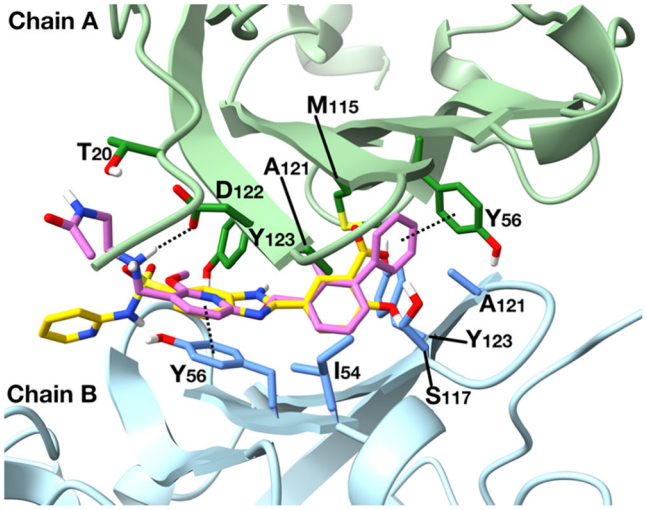

FIGURE 3 The putative binding mode of **10** (golden sticks) into the programmed cell death protein 1 ligand 1 (PD-L1) structure overlapped with the crystal structure of **1** (magenta sticks, PDB Code: 5J89). The protein is shown as a light green (Chain A) and light blue (Chain B) cartoon with interacting residues as sticks. Polar hydrogens only are shown for clarity purposes.

proper ionic interaction with the $_A$Asp122 and thus may represent another point of modification. Herein, according to these observations, a small series of analogs of **10** have been synthesized (**17**–**21**, Table 2). In the novel derivatives, the 2-methylbiphenyl moiety, an essential fragment for interaction with PD-L1, was introduced at position 2 of the benzimidazole central core while the pyridine-sulfonamide group was replaced with a small range of diverse polar side chains, linear or within a cycle, that were demonstrated to increase the potency of **1**.[9] As a negative control, compound **22**, featuring a 1,1'-biphenyl-4-yl substituent in place of the pivotal twisted biphenyl moiety, was prepared.

Compound **10** was prepared as depicted in Scheme 1, according to our previously reported procedures.[21] Briefly, 4-amino-3-nitrobenzene-sulfonyl chloride **23**[22] was reacted with 2-aminopyridine, using pyridine as a solvent at 0°C, to give the corresponding benzenesulfonamide **24**. Subsequent palladium-catalyzed hydrogenation furnished the 3,4-diaminobenzenesulfonamide **25**. Condensation with aldehyde **26**, in dry dimethylformamide (DMF) at 100°C, furnished the benzimidazole compound **27** which, after hydrolysis with lithium hydroxide, yielded target compound **10**.

The synthetic route for the preparation of compounds **17**–**22** is depicted in Scheme 2. Reduction of 3,4-dinitrobenzoic acid **28** into the corresponding alcohol **29**, in the presence of $AlCl_3$ and $NaBH_4$ in dry tetrahydrofuran (THF) and subsequent palladium-catalyzed hydrogenation furnished (3,4-diaminophenyl)methanol **30**. The cyclocondensation reaction in dry DMF at 100°C of 30 with (1,1'-biphenyl)−4-carboxaldehyde or with 2-methyl-(1,1'-biphenyl)−3-carboxaldehyde furnished the 6-hydroxymethyl benzimidazole derivatives **31** and **32**, respectively, which were converted into the corresponding aldehydes **33** and **34** by Dess Martin periodinane oxidation. Finally, reductive alkylation with the appropriate amines yielded the target compounds. For derivatives **17**, **18**, **22**, and **35**, $NaBH_4$ was used as a reducing agent. On the other hand, for amino acid derivatives **20** and **21**, reductive alkylation required $NaBH_3CN$ and a catalytic amount of acetic acid (AcOH) in dry DMF. Hydrolysis of the methyl ester **35** gave the carboxylic acid derivative **19**.

2.4 | In vitro anti-PD-1/PD-L1 activity

The newly synthesized compounds were tested for their ability to inhibit PD-1/PD-L1 interaction using the well-established HTRF assay.[14,34,36,37] Data presented in Table 2 (Supporting Information S1: Figure S3) supported our design strategy. Indeed, the novel derivatives **17**–**21**, exhibited low micromolar IC_{50}. Compound **17**, featuring an ammino ethanolic chain, turned out to be the best-performing compound of the series having an IC_{50} submicromolar. As expected, **22**, is completely inactive and was indeed synthetized as a negative control. These results indicate that benzimidazole-based compounds could be recognized as valuable novel hits for PD-1/PD-L1 inhibition.

2.5 | NMR and computational studies of the 17/PD-L1 complex

2D ^{1}H-^{15}N HSQC NMR experiments were performed to obtain information about the binding region of the complex PD-L1/**17**. To this aim, the variation in signal intensity for the protein (PD-L1, amino acids 18–134) in 2D ^{1}H–^{15}N HSQC spectra was monitored in the presence of 50 μM of **17** (protein:ligand ratio equal to 1:2 considering PD-L1 as dimer). A decrease in signal intensities of the protein is diagnostic of a ligand-induced perturbation. The residues exhibiting the largest intensity changes are highlighted in blue (Figure 4). In particular, upon the addition of the ligand, the cross-peaks of the free protein in the 2D ^{1}H-^{15}N HSQC spectrum decrease in the 55–59 and 118–124 amino acid ranges. These regions include both residues known to directly interact with small molecule inhibitors (such as Tyr56), and part of the hydrophobic residues typically involved in a cage surrounding them (Ile_{54}, Ser_{117}). Interestingly, amino acids are not likely to interact with the ligand but are known to stabilize the PD-L1 homodimer by establishing interchain contacts (Asp_{58}, Arg_{113}) at the interface,[29] showing reduced intensity. These NMR results suggest that **17** has a binding surface of PD-L1 almost overlapping with that of **1**.[14,29]

With the aim to rationalize the newly provided structure-activity relationships data (Table 2), molecular docking simulations of **17** with PD-L1 were carried out (Figure 5, left panel) and a comparison with **1** was provided (Figure 5, right panel). The protein structure cocrystallized with **1** (PDB Code: 5J89)[30] was employed for our simulations. A substantial pose convergence was predicted from our calculations, enforcing the reliability of the design strategy. In particular, **17** makes a T-shape π–π stacking interaction with $_A$Tyr56 (biphenyl moiety) and a π–π stacking interaction with $_B$Tyr$_{56}$ (benzimidazole ring). The critical role of Tyr56 due to its involvement

TABLE 2 Chemical structure of compounds **17**–**22** and inhibitory activity against PD-1/PD-L1 interaction.

Compd. No.	Structure	IC_{50} (μM)
17	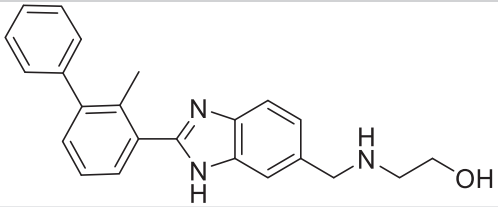	0.79 (±0.30)
18	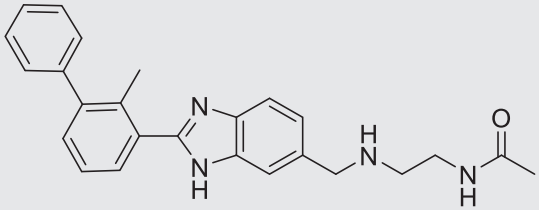	3.16 (±0.07)
19	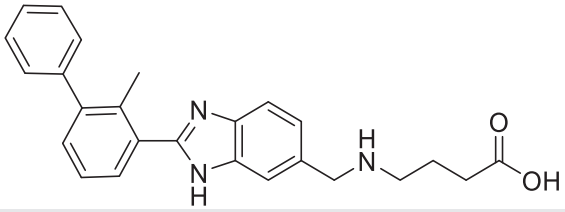	N.D[a]
20	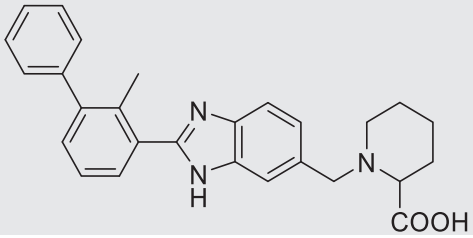	2.48 (±0.34)
21	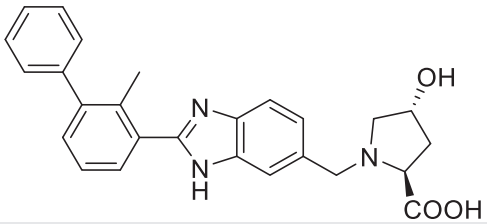	6.95 (±0.95)
22	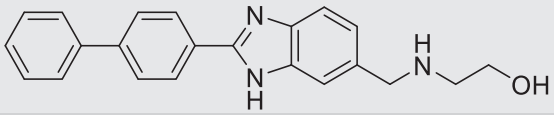	N.A.[b]

Abbreviations: N.A., not available; N.D., not determined; PD-1/PD-L1, programmed cell death protein 1/programmed cell death protein 1 ligand 1.

[a]Not determined because of artifacts related to solubility issues.

[b]Not available, IC_{50} is outside the range of doses.

in specific interactions with **17** through both chains and enlightened by our docking simulations, is in excellent agreement with NMR results showing that its 2D ^{1}H-^{15}N HSQC intensity is importantly reduced. Moreover, our computational study unveils that **17** is surrounded by the hydrophobic residues $_{A,B}$Ile54, $_{A,B}$Met115, $_{A,B}$Ala121 and by $_{A,B}$Ser117 belonging to one of the two mostly perturbed regions found in the NMR experiment. Regarding the polar side chain, it is differently oriented with respect to that of **1** being involved in interactions with $_{A}$Asp122 (even supported by our NMR data) through the amine group, and with $_{A}$Lys124 through the hydroxyl group.

Our new combined NMR and computational results suggest that other chemical modifications to the polar side chain of **17** are needed to enforce the interactions with the PD-L1 binding surface.

Together, these data suggest the promising role of benzimidazole in the development of PD-L1 ligands. Indeed, we have shown that this aromatic system can properly orient the interacting side chains while forming itself important contacts with target proteins. As confirmed by systematic reports on the pharmacological profile of benzimidazole, fine-tuning the substituents on this scaffold can lead to a large effect on potency, activity, and selectivity. Thus **17** has the chance to be further improved in its IC_{50}.

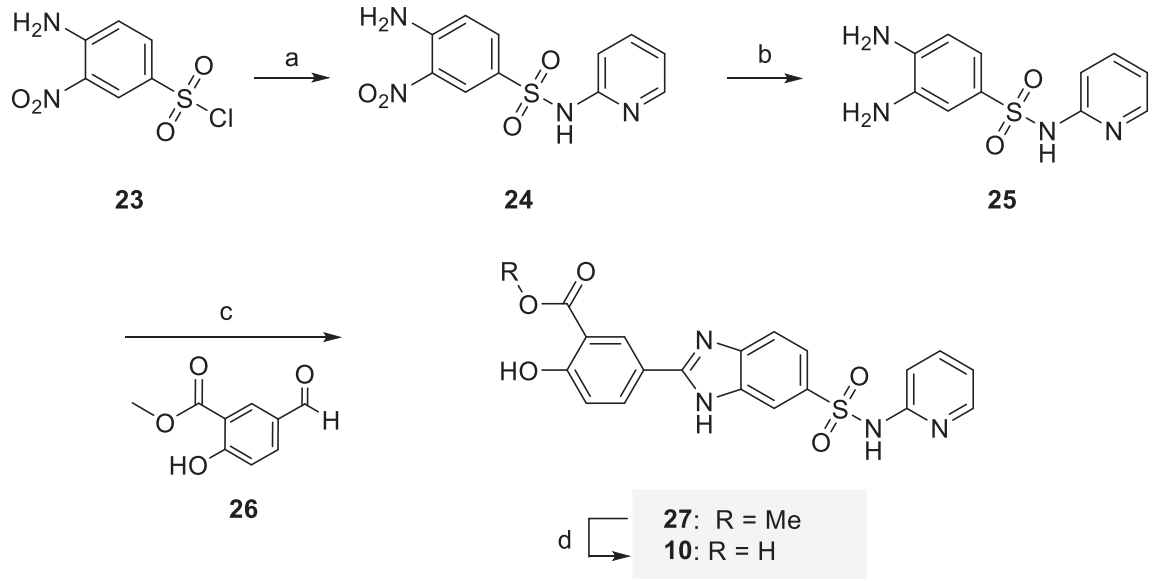

SCHEME 1 Synthesis of compound **10**. Reagents and conditions: (a) pyridine, 0°C to r. t., 2 h (40%); (b) H_2, Pd/C, EtOH, r. t., 12 h (97%); (c) $Na_2S_2O_5$, dry DMF, 100°C, 12 h (80%); (d) LiOH, tetrahydrofuran (THF)/H_2O 4:1, r. t., 12 h (97%).

2.6 | Solubility assay and in silico ADME prediction

Solubility has a crucial role not only in the late phase of drug development but also in the hit identification stage.[38] Insoluble compounds are likely to give assay artifacts and solubility issues could be related to false positive or false negative results. For this reason, before testing the new derivatives, we determined the solubility profile of the compounds in aqueous solutions with 0.2% DMSO by performing nephelometric measurements. We tested three concentrations (10, 50, and 100 µM) within a time frame (0, 24, and 48 h) to properly plan also the scheduled experiments in a cellular contest.

As shown in Figure 6, all compounds displayed good solubility at all the concentrations tested, with the only exception of compound **19** which is not soluble at 100 µM.

Also, the physicochemical characteristics of a drug molecule are pivotal factors that significantly impact its pharmacokinetic profile. To check the drug-likeliness properties of our best compound **17**, the in-silico absorption, distribution, metabolism, excretion (ADME) calculation was done using Qikprop utility (QikProp, Schrödinger, LLC, 2023). The pharmacokinetic profile was checked and the druggability of the molecule was assessed together with that of the reference compound **1**.

The results obtained are shown in Table 3. Various parameters were taken into account such as molecular weight (MW), Lipinsky's rule of 5, rule of 3, partition coefficient, metabolism, H-bond (HB) donor, HB acceptor. The obtained values indicated that **17**, as well as **1**, display good ADME properties orally with a good tolerance rate for oral absorption. The molecules were not violating the Lipinsky's rule of 5 and rule of 3 indicating the druggable properties of the molecules.

3 | CONCLUSIONS

In conclusion, this study showcases a comprehensive approach combining ligand-based and receptor-based VS with NMR spectroscopy for the discovery of small molecules targeting the PD-1/PD-L1 pathway. By employing this strategy, the benzimidazole hit **10** was identified as a promising candidate, possessing a privileged scaffold, and exhibiting a certain (low) binding affinity to PD-L1. Subsequently, a rational lead optimization approach was undertaken, leading to the synthesis of analog **17**. This derivative demonstrated enhanced potency and solubility compared to its precursor. The successful first round of optimization about benzimidazole-based small molecules represents a significant step forward in the development of novel, soluble PD-L1 inhibitors. Based on our NMR-based binding mode of **17**, a second round of synthesis may be envisaged to increase the potency of our derivatives which would allow a full exploration of in-cell efficacy and potential synergistic strategies with monoclonal antibodies, or other drugs might be investigated. Ultimately, the double VS coupled with NMR furnish, besides **10**, novel scaffolds, available to the scientific community, on which to work.

4 | EXPERIMENTAL

4.1 | Virtual screening

4.1.1 | DB preparation

The commercial chemical DB ZINC12 "Leads Now," containing about 2 million compounds, was processed through redundancy checking

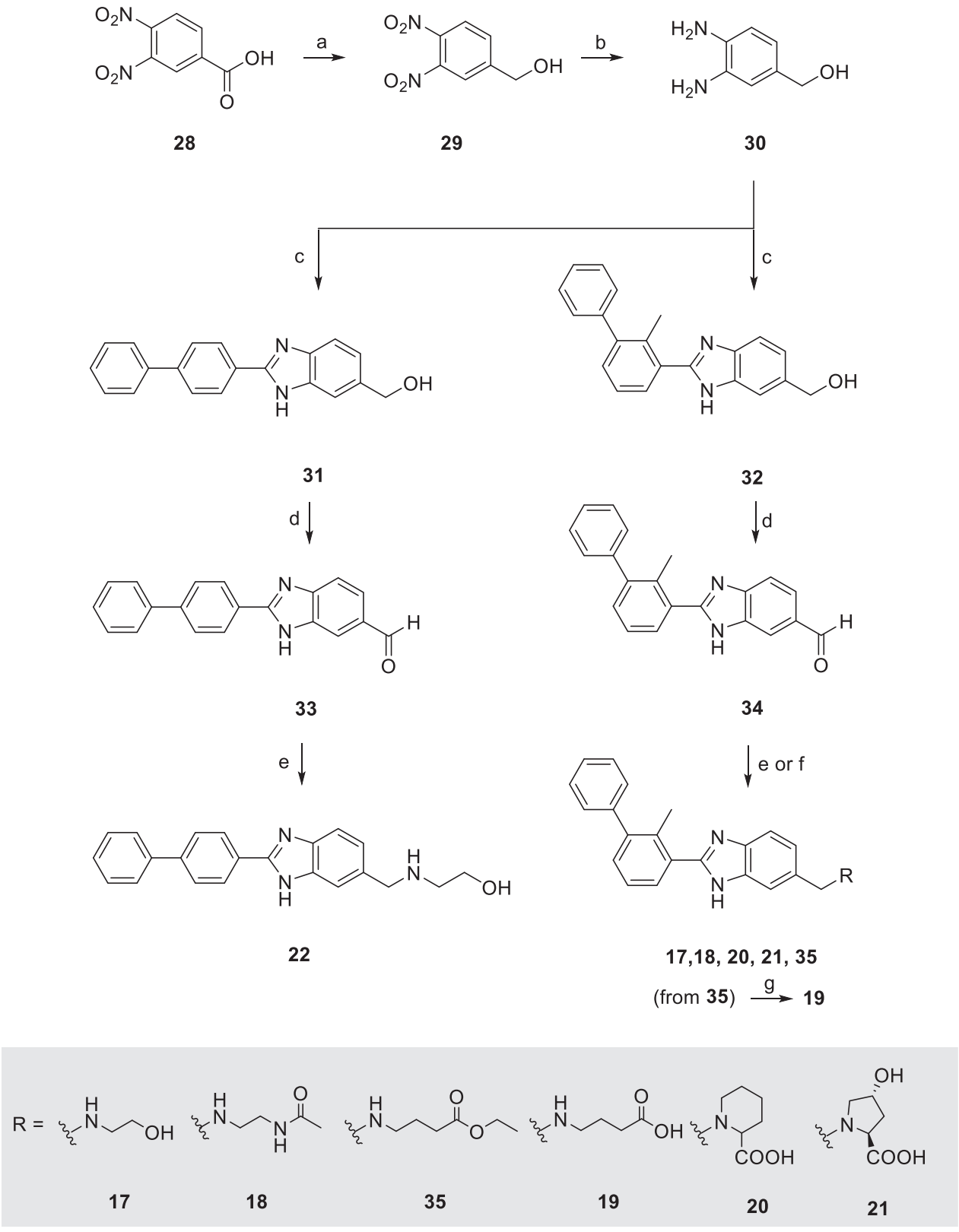

SCHEME 2 Synthesis of compound **17**–**22**. Reagents and conditions: (a) $AlCl_3$, $NaBH_4$, dry THF, r. t., 1 h—reflux, 2 h (57%); (b) H_2, Pd/C 10%, MeOH, r. t., 3 h (99%); (c) (1,1′-biphenyl)−4-carboxaldehyde or 2-methyl-(1,1′-biphenyl)−3-carboxaldehyde, $Na_2S_2O_5$, dry DMF, 100°C, 12 h (60%–72%); (d) Dess-Martin periodinane, dry DCM, r. t., 2 h (50%–75%); (e) (for compounds **17**, **18**, **22**, and **35**) proper amine, $NaBH_4$, dry MeOH, r. t., 2.5 h (70%–82%); (f) (for compounds **20** and **21**) piperidine-2-carboxylic acid or (2*S*,4*R*)−4-hydroxypyrrolidine-2-carboxylic acid, AcOH (cat.), $NaBH_3CN$, dry DMF, 80°C, 3 h (35%–36%); (g) LiOH, THF/H_2O 4:1, r. t., 12 h (97%).

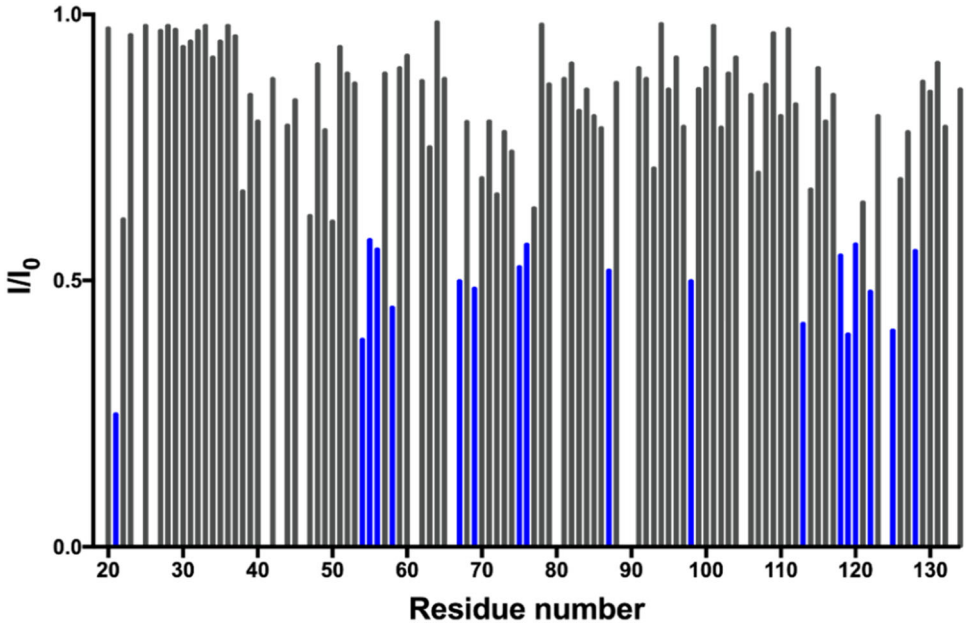

FIGURE 4 Graphical representation of the per-residue intensity changes for programmed cell death protein 1 ligand 1 (PD-L1) in the presence of **17** (50 μM). The residues exhibiting the highest decreases in signal intensities have been colored in blue.

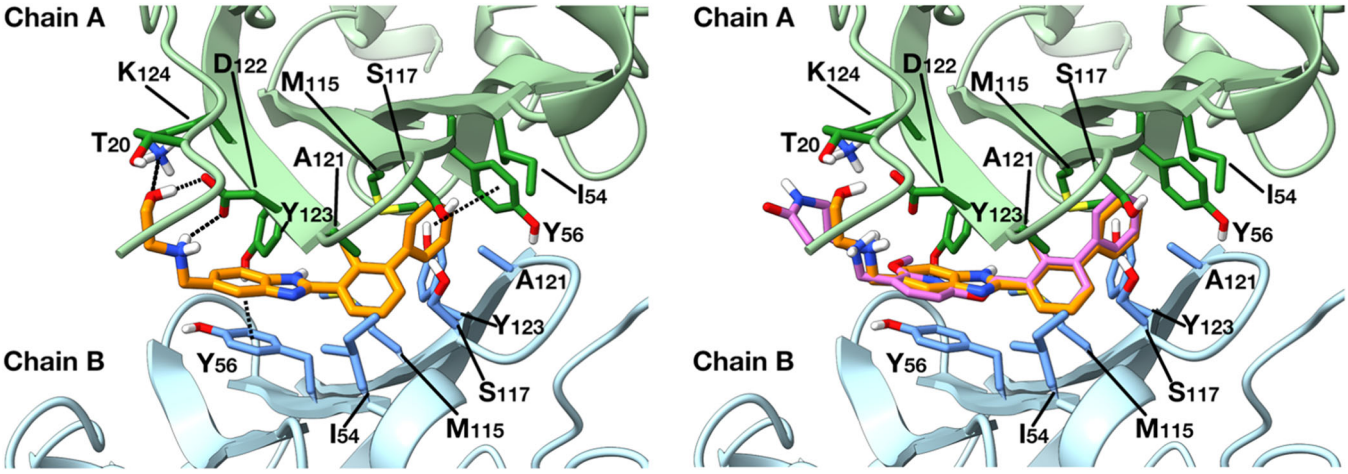

FIGURE 5 Schematic representation of the lowest energy pose of the **17**/programmed cell death protein 1 ligand 1 (PD-L1) complex from molecular docking simulations alone (left panel) and overlapped with the crystal structure of **1**/hPDL1 (right panel, PDB Code: 5J89). **17** and **1** are represented as orange and magenta sticks, respectively. Residues included in the binding site are highlighted in green (Chain A) and azure (Chain B) sticks, residues whose two-dimensional (2D) ^{1}H-^{15}N HSQC signal is reduced in intensity and belonging to the binding site are highlighted in blue sticks, while the rest of the protein is shown as light green (Chain A) and light blue (Chain B) cartoon. Polar hydrogens only are shown for clarity purposes.

and Lipinski filters to select compounds provided with better druglike properties. The obtained ZINC molecules together with those coming from our in-house DB (other 4000 molecules),[20] were prepared using LigPrep[39] with Epik.[40] Conformational sampling was performed on all DB molecules using the ConfGen search algorithm.[41] Using Phase,[42] the DB was indexed with the automatic creation of pharmacophoric sites for each conformer to allow rapid DB alignment and screening.

4.1.2 | Pharmacophore-based VS

Based on our expertise in pharmacophore building,[43,44] a simplified version of our docking-based pharmacophore model[29] was obtained with Phase (see Supporting Information S1: Figure S1). The distance matching tolerance was set to 2.0 Å as a balance between stringent and loose-fitting matching alignment. Screening molecules were required to match four out of four sites. Only those compounds possessing all four

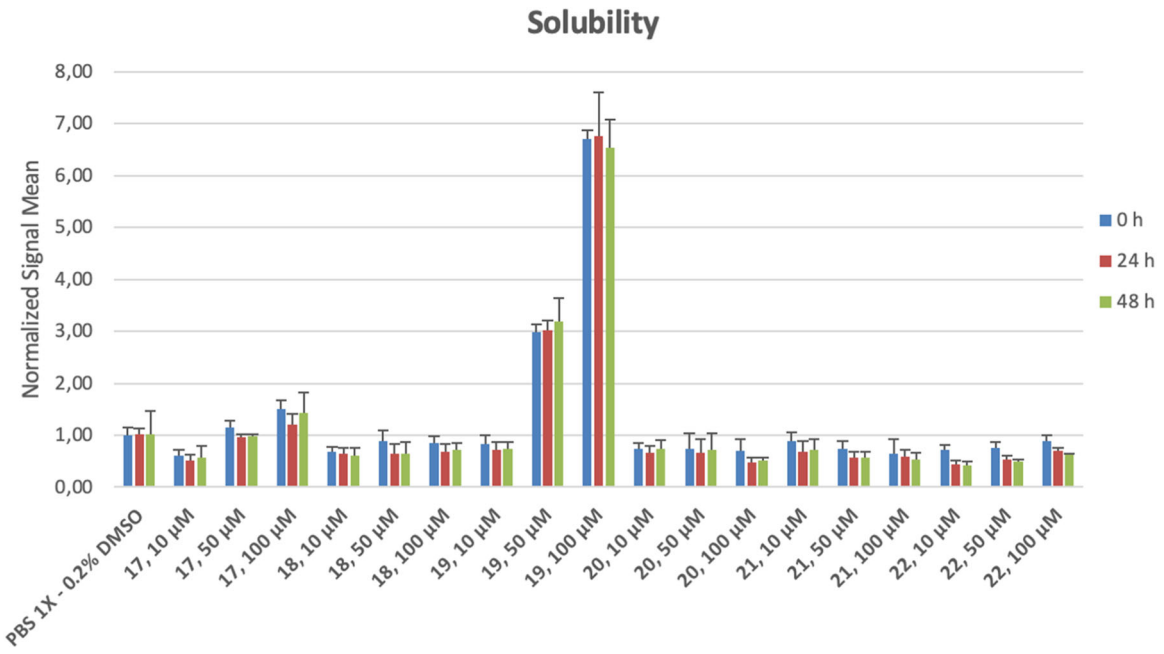

FIGURE 6 Solubility determination (nephelometry). The solubility of the compounds was determined using the instrument Nepheloskan Ascent® (Labsystems). The experiments were conducted at room temperature in a 96-well plate with a final volume of 300 µL. Each compound was tested in triplicate at the concentrations of 10, 50, and 100 µM in phosphate-buffered saline (PBS) with 0.2% DMSO. The measurements were performed at three different times (0, 24, 48 h) from the preparation of the samples. Data obtained were compared with control (PBS with 0.2% DMSO) and the ratio sample/control was determined for each compound. The compounds are considered soluble if the ratio is ≤3.

TABLE 3 Calculated pharmacokinetic properties of compound **17** and the reference compound **1**.

	Comp 1	Comp 17	Lipinski's rule of 3 ranges	Jorgensen rule of 3 ranges	Qikprop ideal ranges
MW	419.522	357.454	<500		130 < *x* < 725
HBD	2	3	0 < *x* < 5		0 < *x* < 6
HBA	5	4.7	0 < *x* < 10		2 < *x* < 20
$\log P_{o/w}$	4.544	3.895	<5		−2 < *x* < 6.5
$\log_S$	−4.354	−4.868		*x*>−5.7	−6.5 < *x* < 0.5
Caco permeability	168.840	314.762		*x*>22	<25 poor; >500 great
#metab	6	4		<7	1 < *x* < 8
PSA	74.233	61.591			7–200
% Human oral absorption	93.420	94.458			

Abbreviations: HBA, H-bond acceptor; HBD, H-bond donor; MW, molecular weight; PSA, polar surface area.

pharmacophoric sites were considered for subsequent receptor-based VS.

4.1.3 | Receptor-based VS

As for the protein, among the human PD-L1 X-ray structures available at the time of the experiments, we chose the PD-L1 dimer structure in complex with the molecule BMS-202, with the PDB code 5J89.[30] The PDB structure was prepared by employing the graphical interface of the Schrödinger's molecular modeling platform, Maestro[45] v. 12.7.156. In particular, the protein was prepared with the Protein Preparation Wizard,[46,47] included in Maestro. Hydrogen atoms were added and missing side chains were filled in by using the Prime[48] module, while crystallographic water molecules were deleted. The N-terminal and C-terminal residues were capped with the acetyl (ACE) and N-methyl amide (NME) groups, respectively. To properly describe the protonation state of the protein residues and to also describe the hydrogen bonding networks correctly at neutral pH, the protonation states were assigned evaluating their pK_a with the Propka[49] program included in Maestro. An inspection of the histidines microenvironment was

performed, given the labile equilibrium at neutral pH of this residue, and none of it was considered to be protonated. Finally, a relaxation procedure was performed by running a restrained minimization only on the initially added hydrogen atoms according to the OPLS2005[50] force field. A receptor grid of 30 Å × 30 Å × 30 Å was computed for the PD-L1 structure around the centroids of the cocrystallized ligand BMS-202. During the grid calculation, the cocrystallized ligand BMS-202 was deleted from the three-dimensional (3D) structure. Docking simulations were performed using the Glide SP[51-53] software included in Maestro using default parameters. Sampling of nitrogen atom inversions (when not belonging to cycles) and of different ring conformations were allowed, while nonplanar amide conformations were penalized. In the simulations, the receptor was kept fixed, while the ligand is treated as flexible. Docking converged to a well-defined binding mode; indeed, an almost complete overlap of the ligand was possible for the best 20 predicted poses.

4.1.4 | Docking calculations

As for compound **17**: the molecule was built and prepared through the LigPrep[39] module of Maestro, employing the OPLS2005 force field. Epik[40,54] was used to evaluate the ligands' pKa at neutral pH and so to properly describe its protonation state. Then, the obtained ligand was optimized at the molecular mechanics level through the MacroModel[55] program included in the Schrödinger suite of programs. For the docking procedure, the grid described above was employed and the simulations performed with Glide SP[49-51] as well. All the presented figures were obtained using ChimeraX[56] and assembled by the means of Gimp (2.10.22 revision 3).

4.2 | NMR experiments

4.2.1 | Protein expression and purification

The proteins were expressed and purified as described previously by us[29] using the drop-wise dilution method of refolding. Briefly, protein was expressed in *Escherichia coli* BL21 (DE3) strain as inclusion bodies which were collected by centrifugation, washed, and dissolved using the 6 M guanidine hydrochloride buffer. The solubilized inclusion bodies being added in four portions to the refolding buffer: 0.1 M Tris pH 8.0, 1 M L-Arg hydrochloride, 2 mM ethylenediaminetetraacetic acid (EDTA, 0.25 mM oxidized glutathione, and 0.25 mM reduced glutathione. Refolded PD-L1 was dialyzed three times over 48–72 h against buffer containing 10 mM Tris pH 8.0 and 20 mM NaCl. Finally, the protein was concentrated and loaded to a size exclusion chromatography column HiLoad 26/600 Superdex 75 (GE Healthcare) preequilibrated with PBS pH 7.4 buffer and concentrated to obtain samples for NMR measurements.

4.2.2 | NMR Spectroscopy

For NMR measurements, the buffer was exchanged by gel filtration to PBS pH 7.4 (PD-L1). Samples of 0.23 mM concentration of PD-L1 were measured in 3 mm NMR tubes and 10% (v/v) of D2O were added to the samples to provide the lock signal. NMR experiments were performed at 300 K on a Bruker 600 MHz Avance III spectrometer equipped with a cryogenically cooled proton-optimized TCI probe. The interaction of the compounds with PD-L1 was evaluated by monitoring the perturbations in chemical shifts of NMR resonances in the ^{1}H-^{15}N 2D SOFAST HMQC[57] upon titration with the compound. NMR spectra were processed with Topspin 3.2 (Bruker) (see the Supporting Information for the resulting spectra).

4.3 | Chemistry

4.3.1 | General directions

All chemicals, purchased from Merck KGaA and Fluorochem Ltd., were of the highest purity. All solvents were reagent grade and, when necessary, were purified and dried by standard methods. All reactions requiring anhydrous conditions were conducted under a positive atmosphere of nitrogen in oven-dried glassware. Standard syringe techniques were used for the anhydrous addition of liquids. Reactions were routinely monitored by thin-layer chromatography (TLC) performed on aluminum-backed silica gel plates (Merck KGaA, Alufolien Kieselgel 60 F254) with spots visualized by UV light (λ = 254, 365 nm) or using a $KMnO_4$ alkaline solution. Solvents were removed using a rotary evaporator operating at a reduced pressure of ~10 Torr. Organic solutions dried over anhydrous Na_2SO_4. Chromatographic purification was done on an automated flash-chromatography system (Isolera™ Dalton 2000, Biotage) using cartridges packed with KP-SIL, 60 Å (40–63 µm particle size). Analytical high-performance liquid chromatography (HPLC) was performed on a Shimadzu SPD 20 A UV/VIS detector (λ = 220 and 254 nm) using C-18 column C18 Phenomenex LunaPolar 100 Å (100 × 4.60 mm; 5 µm) at 25°C using a mobile phase A (water + 0.05% trifluoracetic acid [TFA]) and B (ACN + 0.03% TFA) at a flow rate of 1.25 mL/min. Preparative HPLC was performed using an Shimadzu Prominence LC-20AP with the UV detector set to 220 and 254 nm. Samples were injected onto a Phenomenex Synergi Fusion–RP 80 A (150 × 21 mm; 4 µm) C18 column at room temperature. Mobile phases of A (water + 0.05% TFA) and B (ACN + 0.03% TFA) were used with a flow rate of 20 mL/min. A general gradient of 0–3 min at 5% B, 3–14 min increasing from 5% to 35% B, and 14–18 min increasing from 35% to 90% B was used, followed by a 90% B flush for another 2 min. Small variations in this purification method were made as needed to achieve ideal separation for each compound. ^{1}H spectra were recorded at 400 MHz on a Bruker Ascend 400 spectrometer while ^{13}C NMR spectra were obtained by distortionless enhancement by polarization transfer quarternary (DEPTQ) spectroscopy on the same spectrometer. Chemical shifts

are reported in δ (ppm) relative to the internal reference tetramethylsilane (TMS). Due to the existence of tautomers, some ^{1}H and ^{13}C NMR signals could not be detected for some of the prepared benzimidazoles so only the distinct signals were reported. Low-resolution mass spectra were recorded on a Finnigan LCQ DECA TermoQuest mass spectrometer in electrospray positive and negative ionization modes (ESI-MS). High-resolution mass spectra were recorded on a ThermoFisher Scientific Orbitrap XL mass spectrometer in electrospray positive ionization modes (ESI-MS). All tested compounds possessed a purity of at least 95% established by HPLC unless otherwise noted.

The InChI codes of the investigated compounds, together with some biological activity data, are provided as Supporting Information.

4.3.2 | Compound synthesis and characterization

2-Hydroxy-5-{6-[*N*-(pyridin-2-yl)sulfamoyl]−1*H*-benzo[*d*]imidazol-2-yl}benzoic acid (**10**): To a solution of **27** (195 mg, 0.46 mmol) in a mixture of THF/H_2O (4:1) (8 mL) was added LiOH (44.0 mg, 1.80 mmol). The mixture was stirred at room temperature for 12 h and then treated with HCl (1 N) to pH 3. The solution was extracted with EtOAc (3 × 30 mL), and the combined organic phases were washed with brine (10 mL), dried (Na_2SO_4), filtered, and concentrated in vacuo. Purification by column chromatography on silica gel (dichloromethane [DCM]−EtOAc) provided the title compound (183 mg, 97%) as a white solid. ^{1}H NMR (400 MHz, DMSO-d_6): δ 8.72 (d, *J* = 2.3 Hz, 1H), 8.38 (dd, *J* = 8.8, 2.3 Hz, 1H), 8.15 (d, *J* = 1.6 Hz, 1H), 8.05–8.00 (m, 1H), 7.89–7.83 (m, 1H), 7.83–7.78 (m, 1H), 7.78–7.66 (m, 1H), 7.30–7.16 (m, 2H), 6.92–6.78 (m, 1H). ^{13}C NMR (101 MHz, DMSO-d_6) δ 170.84, 163.91, 153.21, 151.81, 140.73, 134.27, 130.44, 122.42, 118.55, 114.50, 114.40, 113.90, 113.33. HRMS (ESI): *m/z* $[M+H]^+$ calcd. for $C_{19}H_{14}N_4O_5S+H^+$: 411.0758. Found: 411.0756.

2-({[2-(2-Methyl-[1,1'-biphenyl]−3-yl)−1*H*-benzo[*d*]imidazol-6-yl]methyl}amino)ethan-1-ol (**17**): To a solution of compound 34 (50 mg, 0.16 mmol) in dry MeOH (3.0 mL) was added 2-aminoethanol (10 µL, 0.16 mmol) under a nitrogen atmosphere. The solution was stirred at room temperature for 2.5 h. After cooling at 0°C, $NaBH_4$ was added portion-wise until disappearance of the intermediate imine (TLC analysis). The reaction mixture, after the addition of water (20 mL), was concentrated in vacuo and extracted with EtOAc (3 × 40 mL). The combined organic phases were washed with a saturated solution of $NaHCO_3$ (3 × 20 mL) and brine (10 mL), dried, filtered, and concentrated in vacuo to yield the title compound (42 mg, 73%) as a white solid. ^{1}H NMR (400 MHz, Methanol-d_6) δ 7.63 (s, 1H), 7.61–7.56 (m, 2H), 7.48–7.42 (m, 2H), 7.41–7.34 (m, 5H), 7.31 (dd, *J* = 8.3, 1.6 Hz, 1H), 3.97 (s, 2H), 3.70 (t, *J* = 5.6 Hz, 2H), 2.80 (t, *J* = 5.6 Hz, 2H), 2.29 (s, 3H). ^{13}C NMR (101 MHz, Methanol-d_6) δ 154.81, 145.03, 143.02, 135.94, 132.69, 132.50, 130.26, 129.35, 128.29, 126.85, 124.77, 61.25, 54.50, 51.44, 18.66. HRMS (ESI): *m/z* $[M+H]^+$ calcd. for $C_{23}H_{23}N_3O+H^+$: 358.1914. Found: 358.1909.

N-[2-({[2-(2-Methyl-[1,1'-biphenyl]−3-yl)−1*H*-benzo[*d*]imidazol-6-yl]methyl}amino)ethyl]acetamide (**18**): Compound **18** (52 mg, 75%) was obtained as a white solid from derivative 34 (54 mg, 0.17 mmol) and *N*-(2 aminoethyl)acetamide (16 mL, 0.17 mmol) according to the procedure described for 17. ^{1}H NMR (400 MHz, Methanol-d_6) δ 7.62 (s, 1H), 7.58 (dd, *J* = 7.3, 1.9 Hz, 1H), 7.49–7.41 (m, 3H), 7.42–7.33 (m, 5H), 7.31 (dd, *J* = 8.2, 1.6 Hz, 1H), 3.96 (s, 2H), 3.36 (t, *J* = 6.4 Hz, 2H), 2.79 (t, *J* = 6.4 Hz, 2H), 2.29 (s, 3H), 1.94 (s, 3H). ^{13}C NMR (101 MHz, Methanol-d_6) δ 173.72, 154.84, 145.03, 143.00, 135.93, 132.67, 132.50, 130.29, 129.35, 128.29, 126.85, 124.78, 54.27, 48.85, 39.62, 22.58, 18.66. HRMS (ESI): *m/z* $[M+H]^+$ calcd. for $C_{25}H_{26}N_4O+H^+$: 399.2179. Found: 399.2178.

4-({[2-(2-Methyl-[1,1'-biphenyl]−3-yl)−1*H*-benzo[*d*]imidazol-6-yl]methyl}amino)butanoic acid (**19**): Compound **19** (45 mg, 97%) was obtained as a white solid from derivative 35 (50 mg, 0.12 mmol) according to the hydrolysis procedure described for **10**. ^{1}H NMR (400 MHz, Methanol-d_6) δ 7.67–7.54 (m, 3H), 7.49–7.43 (m, 2H), 7.42–7.34 (m, 5H), 7.27–7.19 (m, 1H), 4.61 (s, 2H), 3.39 (t, *J* = 8.1 Hz, 2H), 2.47 (t, *J* = 8.1 Hz, 2H), 2.30 (s, 3H), 2.11–1.98 (m, 2H). ^{13}C NMR (101 MHz, Methanol-d_6) δ 175.96, 153.93, 145.72, 142.06, 136.47, 130.72, 130.23, 129.57, 128.75, 128.32, 127.65, 126.78, 117.57, 116.01, 114.88, 112.62, 64.54, 52.21, 31.58, 22.45, 18.49. HRMS (ESI): *m/z* $[M+H]^+$ calcd. for $C_{25}H_{25}N_3O_2+H^+$: 400.2020. Found: 400.2019.

1-{[2-(2-Methyl-[1,1'-biphenyl]−3-yl)−1*H*-benzo[*d*]imidazol-6-yl]methyl}piperidine-2-carboxylic acid (**20**): To a solution of compound **34** (53 mg, 0.17 mmol) in dry DMF (2.0 mL), piperidine-2-carboxylic acid (66 mg, 0.51 mmol), $NaBH_3CN$ (32 mg, 0.51 mmol) and a drop of AcOH were added under a nitrogen atmosphere. Purification by reverse phase high−performance liquid chromatography (RP-HPLC) provided the title compound (25 mg, 35%) as a white solid. ^{1}H NMR (400 MHz, Methanol-d_6) δ 8.02–7.99 (m, 1H), 7.89 (d, *J* = 8.4 Hz, 1H), 7.73–7.66 (m, 2H), 7.58–7.53 (m, 2H), 7.52–7.47 (m, 2H), 7.46–7.34 (m, 3H), 4.85–4.81 (m, 2H), 4.46–4.31 (m, 1H), 4.11–3.99 (m, 1H), 3.64–3.49 (m, 1H), 3.20–3.07 (m, 1H), 2.32 (s, 3H), 2.00–1.83 (m, 3H), 1.79–1.61 (m, 2H). ^{13}C NMR (101 MHz, Methanol-d_6) δ 171.77, 154.48, 145.67, 142.15, 136.40, 136.26, 134.57, 130.64, 130.24, 129.55, 129.22, 128.71, 128.03, 127.57, 127.24, 119.25, 115.99, 60.69, 52.46, 28.97, 23.29, 22.30, 18.51. HRMS (ESI): *m/z* $[M+H]^+$ calcd. for $C_{27}H_{27}N_3O_2+H^+$: 426.2176. Found: 426.2173.

(2*S*,4*R*)−4-Hydroxy-1-{[2-(2-methyl-[1,1'-biphenyl]−3-yl)−1*H*-benzo[*d*]imidazol-6-yl]methyl}pyrrolidine-2-carboxylic acid (**21**): Compound **21** (29 mg, 36%) was obtained as a white solid from derivative **34** (59 mg, 0.19 mmol) and (2*S*,4*R*)−4-hydroxypyrrolidine-2-carboxylic acid (139 mg, 0.57 mmol) according to the procedure described for **20**. ^{1}H NMR (400 MHz, Methanol-d_6) δ 8.05–8.01 (m, 1H), 7.87 (dd, *J* = 8.3, 1.6 Hz, 1H), 7.73–7.67 (m, 2H), 7.59–7.47 (m, 4H), 7.45–7.34 (m, 3H), 4.80 (d, *J* = 12.9 Hz, 1H), 4.67 (d, *J* = 12.9 Hz, 1H), 4.60–4.55 (m, 2H), 3.74 (dd, *J* = 12.5, 4.4 Hz, 1H), 3.46–3.37 (m, 1H), 2.58–2.49 (m, 1H), 2.34 (s, 3H), 2.30–2.20 (m, 1H). ^{13}C NMR (101 MHz, Methanol-d_6) δ 171.43, 154.47, 145.67, 142.17, 136.40, 136.30, 134.54, 130.64, 130.23, 129.55, 128.71, 128.61, 128.55, 127.56, 118.54, 116.12, 70.33, 67.88, 62.80, 62.21, 39.69, 18.50.

HRMS (ESI): *m/z* $[M+H]^+$ calcd. for $C_{26}H_{25}N_3O_3+H^+$: 428.1969. Found: 428.1968.

2-({[2-([1,1'-Biphenyl]−4-yl)−1*H*-benzo[*d*]imidazol-6-yl]methyl}amino)ethan-1-ol (**22**): Compound **22** (47 mg, 82%) was obtained as a white solid from derivative **33** (50 mg, 0.16 mmol) and 2-aminoethanol (10 mL, 0.16 mmol) according to the procedure described for **17**. ^{1}H NMR (400 MHz, Methanol-d_6) δ 8.18 (d, J = 8.4 Hz, 2H), 7.82 (d, J = 8.4 Hz, 2H), 7.74–7.69 (m, 2H), 7.64–7.59 (m, 2H), 7.51–7.45 (m, 2H), 7.42–7.35 (m, 1H), 7.30 (dd, J = 8.3, 1.6 Hz, 1H), 3.95 (s, 2H), 3.71 (t, J = 5.6 Hz, 2H), 2.79 (t, J = 5.6 Hz, 2H). ^{13}C NMR (101 MHz, Methanol-d_6) δ 153.60, 144.37, 141.33, 130.04, 129.80, 128.99, 128.62, 128.29, 128.00, 124.96, 61.27, 54.52, 51.51. HRMS (ESI): *m/z* $[M+H]^+$ calcd. for $C_{22}H_{21}N_3O+H^+$: 344.1757. Found: 344.1750.

4-Amino-3-nitro-*N*-(pyridin-2-yl)benzenesulfonamide (**24**): To a cooled (0°C) stirred solution of **23** (1.41 g, 5.98 mmol) in dry pyridine (6 mL), 2-aminopyridine (506 mg, 5.38 mmol) was added portion wise, under N_2 atmosphere. The reaction was kept at room temperature until the disappearance of the starting material (monitored by TLC). Then, water (10 mL) was added: the resulting solid was filtered and washed with water to afford the title compound (700 mg, 40%) as an orange solid. ^{1}H NMR (400 MHz, DMSO-d_6) δ 8.49–8.39 (m, 1H), 8.09–8.00 (m, 1H), 7.94 (s, 2H, exchangeable with D_2O), 7.78–7.69 (m, 2H), 7.13–7.09 (m, 2H), 6.91–6.83 (m, 1H). MS (ESI) *m/z*: 295 $(M+H)^+$.

3,4-Diamino-*N*-(pyridin-2-yl)benzenesulfonamide (**25**): Pd/C (10 wt% on activated carbon, 0.1 equiv) was added to a solution of **24** (440 mg, 1.50 mmol) in EtOAc (15 mL) and the reaction was stirred under H_2 (1 atm, balloon) for 12 h. The reaction mixture was filtered and concentrated to give the title compound (385 mg, 97%) as light-brown solid. ^{1}H NMR (400 MHz, DMSO-d_6) δ 10.86 (s, 1H, exchangeable with D_2O), 8.13–8.04 (m, 1H), 7.68–7.58 (m, 1H), 7.07 (d, J = 8.5 Hz, 1H), 7.02–6.97 (m, 1H), 6.96–6.85 (m, 2H), 6.48 (d, J = 8.2 Hz, 1H), 5.23 (brs, 2H, exchangeable with D_2O), 4.82 (brs, 2H, exchangeable with D_2O). MS (ESI) *m/z*: 265 $(M+H)^+$.

Methyl 2-hydroxy-5-{6-[*N*-(pyridin-2-yl)sulfamoyl]−1*H*-benzo[*d*]imidazol-2-yl}benzoate (**27**): To a solution of 3,4-diamino-*N*-(pyridin-2-yl)benzenesulfonamide **25** (200 mg, 0.75 mmol) in dry DMF (6.0 mL), methyl 5-formyl-2-hydroxybenzoate **26** (135 mg, 0.75 mmol) and $Na_2S_2O_5$ (187 mg, 0.98 mmol) were added and the resulting mixture was heated at 100°C for 12 h. After cooling at room temperature, water was added. The brown precipitate formed was filtered and washed with water. Compound **27** (255 mg, 80%) was obtained as a light-yellow solid after recrystallization from EtOH. ^{1}H NMR (400 MHz, DMSO-d_6) δ 10.86 (brs, 1H, exchangeable with D_2O), 8.63 (d, J = 2.3 Hz, 1H), 8.29 (dd, J = 8.8, 2.3 Hz, 1H), 8.09 (d, J = 1.6 Hz, 1H), 8.05–7.99 (m, 1H), 7.76–7.61 (m, 3H), 7.19 (dd, J = 8.8, 4.1 Hz, 2H), 6.91–6.82 (m, 1H), 3.96 (s, 3H). MS (ESI) *m/z*: 425 $(M+H)^+$.

(3,4-Dinitrophenyl)methanol (**29**): A solution of $AlCl_3$ (1.66 g, 12.45 mmol) in dry THF (20 mL) was added drop-wise to a stirred suspension of 3,4-dinitrobenzoic acid **28** (2.20 g, 10.37 mmol) and $NaBH_4$ (1.41 g, 37.34 mmol) in dry THF (20 mL) over a period of 20 min. The reaction mixture was stirred for 1 h at room temperature then an additional 2 h at reflux. Upon cooling, the reaction was placed on ice, quenched with 50 mL of HCl (1 N) and extracted with Et_2O (3 × 30 mL). The combined organic phases were washed with brine (50 mL), dried (Na_2SO_4), filtered, and concentrated in vacuo. Purification by column chromatography on silica gel (DCM−MeOH) provided the title compound (1.17 g, 57%) as a yellow solid. ^{1}H NMR (400 MHz, DMSO-d_6): δ 8.21 (d, J = 8.3 Hz, 1H), 8.09 (d, J = 1.7 Hz, 1H), 7.87 (dd, J = 8.3, 1.7 Hz, 1H), 5.75 (t, J = 5.7 Hz, 1H, exchangeable with D_2O), 4.69 (d, J = 5.7 Hz, 2H). MS (ESI) *m/z*: 199 $(M+H)^+$.

(3,4-Diaminophenyl)methanol (**30**): Compound **30** (172 mg, 99%) was obtained as a yellow oil from derivative **29** (250 mg, 1.26 mmol) in MeOH (120 mL) according to the procedure described for **25**. ^{1}H NMR (400 MHz, DMSO-d_6) δ 6.49 (d, J = 1.9 Hz, 1H), 6.44 (d, J = 7.7 Hz, 1H), 6.33 (dd, J = 7.7, 1.9 Hz, 1H), 4.68 (t, J = 5.6 Hz, 1H, exchangeable with D_2O), 4.43–4.33 (brs, 4H, exchangeable with D_2O), 4.23 (d, J = 5.6 Hz, 2H). MS (ESI) *m/z*: 139 $(M+H)^+$.

[2-([1,1'-Biphenyl]−4-yl)−1*H*-benzo[*d*]imidazol-6-yl]methanol (**31**): Compound **31** (194 g, 60%) was obtained as a yellow solid from derivative **30** (150 mg, 1.08 mmol) and [1,1'-biphenyl]−4-carbaldehyde (197 mg, 1.08 mmol) according to the procedure described for **27**. ^{1}H NMR (400 MHz, DMSO-d_6) δ 12.67 (s, 1H, exchangeable with D_2O), 8.34–8.30 (m, 1H), 8.26 (d, J = 8.2 Hz, 2H), 7.87 (d, J = 8.2 Hz, 2H), 7.83–7.75 (m, 2H), 7.57–7.50 (m, 3H), 7.46–7.40 (m, 2H), 5.12 (t, J = 5.8 Hz, 1H, exchangeable with D_2O), 4.58 (d, J = 5.8 Hz, 2H). MS (ESI) *m/z*: 301 $(M+H)^+$.

[2-(2-Methyl-[1,1'-biphenyl]−3-yl)−1*H*-benzo[*d*]imidazol-6-yl]methanol (**32**): Compound **32** (253 mg, 72%) was obtained as a light-yellow solid from derivative **30** (220 mg, 1.12 mmol) and 2-methyl-[1,1'-biphenyl]−3-carbaldehyde (220 mg, 1.12 mmol) according to the procedure described for **27**. ^{1}H NMR (400 MHz, DMSO-d_6) δ 12.57 (s, 1H, exchangeable with D_2O), 7.67 (d, J = 7.6 Hz, 1H), 7.64–7.57 (m, 1H), 7.53–7.42 (m, 3H), 7.45–7.30 (m, 5H), 7.21–7.13 (m, 1H), 5.11 (t, J = 5.8 Hz, 1H, exchangeable with D_2O), 4.59 (d, J = 5.8 Hz, 2H), 2.37 (s, 3H). MS (ESI) *m/z*: 315 $(M+H)^+$.

2-([1,1'-Biphenyl]−4-yl)−1*H*-benzo[*d*]imidazole-6-carbaldehyde (**33**): To a suspension of Dess Martin periodinane (148 mg, 0.35 mmol) in dry DCM (3.3 mL), compound **31** was added and the resulting mixture was stirred at room temperature for 2 h, then filtered and washed with DCM (30 mL). The organic phase was washed with H_2O (3 × 10 mL), dried, filtered, and concentrated in vacuo. Purification by column chromatography on silica gel (DCM−MeOH) provided the title compound (50 mg, 50%) as a white solid. ^{1}H NMR (400 MHz, Methanol-d_6) δ 10.08 (s, 1H), 8.27–8.21 (m, 3H), 7.94–7.85 (m, 3H), 7.79 (d, J = 8.4 Hz, 1H), 7.77–7.71 (m, 2H), 7.55–7.48 (m, 2H), 7.48–7.37 (m, 1H). MS (ESI) *m/z*: 299 $(M+H)^+$.

2-(2-Methyl-[1,1'-biphenyl]−3-yl)−1*H*-benzo[*d*]imidazole-6-carbaldehyde (**34**): Compound **34** (112 mg, 75%) was obtained as a white solid from derivative **32** (150 mg, 0.48 mmol) according to the procedure described for **33**. ^{1}H NMR (400 MHz, Methanol-d_6) δ 10.09 (s, 1H), 8.32–8.16 (m, 1H), 7.97–7.90 (m, 1H), 7.86–7.73 (m, 1H), 7.76 (dd, J = 7.1, 2.0 Hz, 1H), 7.51–7.46 (m, 3H), 7.46–7.35 (m, 4H), 2.35 (s, 3H). MS (ESI) *m/z*: 313 $(M+H)^+$.

Ethyl 4-({[2-(2-methyl-[1,1'-biphenyl]−3-yl)−1*H*-benzo[*d*]imidazol-6-yl]methyl}amino)butanoate (**35**): Compound **35** (56 mg, 74%) was obtained as a light-yellow solid from derivative **34** (55 mg, 0.18 mmol) and ethyl 4-aminobutyrate (24 mg, 0.18 mmol) according to the procedure described for **17**. ^{1}H NMR (400 MHz, Methanol-d_6) δ 7.74–7.67 (m 1H), 7.61 (dd, J = 7.3, 1.9 Hz, 1H), 7.52–7.42 (m, 3H), 7.45–7.34 (m, 5H), 7.32 (dd, J = 8.3, 1.6 Hz, 1H), 4.12 (q, J = 7.1 Hz, 2H), 3.94 (s, 2H), 2.71–2.66 (m, 2H), 2.40 (t, J = 7.3 Hz, 2H), 2.32 (s, 3H), 1.95–1.78 (m, 2H), 1.23 (t, J = 7.1 Hz, 3H). MS (ESI) m/z: 428 $(M+H)^+$.

4.4 | Solubility determination

Solubility of the compounds was determined using Nepheloskan Ascent® (Labsystems). The experiments were performed at room temperature in 96-well plates in a final volume of 300 µL. Each compound was tested in triplicate at the concentrations of 10, 50, and 100 µM in PBS1X with 0.2% DMSO. The measurements were performed at three different times (0, 24, 48 h) from the preparation of the samples. Data obtained were compared to control (PBS with 0.2% DMSO) and the ratio sample/control was determined for each compound. The compounds are considered soluble if the ratio is ≤ 3.

4.5 | HTRF assay

The abilities of compounds **17–22** to inhibit PD-1/PD-L1 interaction were determined using the PD-1/PD-L1 HTRF binding assay kit from Cisbio. The experiments were performed according to the manufacturer's guidelines (https://www.cisbio.com/usa/drug-discovery/human-pd1pd-l1-biochemical-interaction-assay). The IC_{50} values for PD-1/PD-L1 inhibition were determined by analyzing the log of the concentration versus response curves using the Origin Software version 7.0.[14]

4.6 | In silico ADME calculations

In the present study molecules **17** and **1** have been processed by QikProp 2.3,[58] which computed 36 properties for each compound. Herein, the physicochemical properties considered are: MW, logP, logS, H bond donor and acceptor, polar surface area, human oral absorption, and Caco-2 cell permeability. These parameters are generally considered in the Rule of 5 anche the Rule of 3. No violations are reported for both compounds.

ACKNOWLEDGMENTS

This research was funded by the Italian Ministry of Education, University, and Research (MIUR), Progetti di Rilevante Interesse Nazionale, PRIN 2017 (2017PHRC8X) and PRIN 2022 (2022YWZWB2). This research was funded (to T.A.H.) by the project POIR.04.04.00-00-420 F/17-00, which is carried out within the TEAM program of the Foundation for Polish Science co-financed by the European Union under the European Regional Development Fund.

CONFLICTS OF INTEREST STATEMENT

The authors declare no conflicts of interest.

ORCID

Greta Donati http://orcid.org/0000-0002-0311-1721
Monica Viviano https://orcid.org/0000-0003-1118-790X
Lukasz Skalniak https://orcid.org/0000-0002-6707-6697
Valeria La Pietra http://orcid.org/0000-0001-8096-8377

REFERENCES

[1] N. A. Carreau, A. C. Pavlick, *Future Oncol.* **2019**, *15*, 349.
[2] L. Sun, L. Zhang, J. Yu, Y. Zhang, X. Pang, C. Ma, M. Shen, S. Ruan, H. S. Wasan, S. Qiu, *Sci. Rep.* **2020**, *10*, 2083.
[3] A. Patnaik, S. P. Kang, D. Rasco, K. P. Papadopoulos, J. Elassaiss-Schaap, M. Beeram, R. Drengler, C. Chen, L. Smith, G. Espino, K. Gergich, L. Delgado, A. Daud, J. A. Lindia, X. N. Li, R. H. Pierce, J. H. Yearley, D. Wu, O. Laterza, M. Lehnert, R. Iannone, A. W. Tolcher, *Clin. Cancer Res.* **2015**, *21*, 4286.
[4] S. L. Topalian, F. S. Hodi, J. R. Brahmer, S. N. Gettinger, D. C. Smith, D. F. McDermott, J. D. Powderly, R. D. Carvajal, J. A. Sosman, M. B. Atkins, P. D. Leming, D. R. Spigel, S. J. Antonia, L. Horn, C. G. Drake, D. M. Pardoll, L. Chen, W. H. Sharfman, R. A. Anders, J. M. Taube, T. L. McMiller, H. Xu, A. J. Korman, M. Jure-Kunkel, S. Agrawal, D. McDonald, G. D. Kollia, A. Gupta, J. M. Wigginton, M. Sznol, *N. Engl. J. Med.* **2012**, *366*, 2443.
[5] J. R. Brahmer, S. S. Tykodi, L. Q. M. Chow, W.-J. Hwu, S. L. Topalian, P. Hwu, C. G. Drake, L. H. Camacho, J. Kauh, K. Odunsi, H. C. Pitot, O. Hamid, S. Bhatia, R. Martins, K. Eaton, S. Chen, T. M. Salay, S. Alaparthy, J. F. Grosso, A. J. Korman, S. M. Parker, S. Agrawal, S. M. Goldberg, D. M. Pardoll, A. Gupta, J. M. Wigginton, *N. Engl. J. Med.* **2012**, *366*, 2455.
[6] A. Constantinidou, C. Alifieris, D. T. Trafalis, *Pharmacol. Ther.* **2019**, *194*, 84.
[7] J. D. Twomey, B. Zhang, *AAPS. J.* **2021**, *23*, 39.
[8] X. Lin, X. Lu, G. Luo, H. Xiang, *Eur. J. Med. Chem.* **2020**, *186*, 111876.
[9] L. S. Chupak, X. Zheng. WO034820A1, 2015.
[10] M. Konieczny, B. Musielak, J. Kocik, L. Skalniak, D. Sala, M. Czub, K. Magiera-Mularz, I. Rodriguez, M. Myrcha, M. Stec, M. Siedlar, T. A. Holak, J. Plewka, *J. Med. Chem.* **2020**, *63*, 11271.
[11] C. Sun, M. Yin, Y. Cheng, Z. Kuang, X. Liu, G. Wang, X. Wang, K. Yuan, W. Min, J. Dong, Y. Hou, L. Hu, G. Zhang, W. Pei, L. Wang, Y. Sun, X. Yu, Y. Xiao, H. Deng, P. Yang, *J. Med. Chem.* **2023**, *66*, 2064.
[12] R. Butera, M. Ważyńska, K. Magiera-Mularz, J. Plewka, B. Musielak, E. Surmiak, D. Sala, R. Kitel, M. de Bruyn, H. W. Nijman, P. H. Elsinga, T. A. Holak, A. Dömling, *ACS Med. Chem. Lett.* **2021**, *12*, 768.
[13] T. Wang, S. Cai, Y. Cheng, W. Zhang, M. Wang, H. Sun, B. Guo, Z. Li, Y. Xiao, S. Jiang, *J. Med. Chem.* **2022**, *65*, 3879.
[14] P. Russomanno, G. Assoni, J. Amato, V. M. D'Amore, R. Scaglia, D. Brancaccio, M. Pedrini, G. Polcaro, V. La Pietra, P. Orlando, M. Falzoni, L. Cerofolini, S. Giuntini, M. Fragai, B. Pagano, G. Donati, E. Novellino, C. Quintavalle, G. Condorelli, F. Sabbatino, P. Seneci, D. Arosio, S. Pepe, L. Marinelli, *J. Med. Chem.* **2021**, *64*, 16020.
[15] J.-J. Park, E. P. Thi, V. H. Carpio, Y. Bi, A. G. Cole, B. D. Dorsey, K. Fan, T. Harasym, C. L. Iott, S. Kadhim, J. H. Kim, A. C. H. Lee, D. Nguyen, B. S. Paratala, R. Qiu, A. White, D. Lakshminarasimhan,

C. Leo, R. K. Suto, R. Rijnbrand, S. Tang, M. J. Sofia, C. B. Moore, *Nat. Commun.* **2021**, *12*, 1222.
[16] E. Aktoudianakis, A. C. Du, M. Graupe, L. T. LAD, P. A. Machicao Tello, J. W. Medley, S. E. Metobo, P. K. Mukherjeed, D. Naduthambi, E. Q. Parkhill, B. W. Phillips, S. Preston Simonovich, N. H. Squires, P. Wang, W. J. Watkins, J. Xu, K. S. Yang, C. A. Ziebenhaus, WO2019160882A1, **2019**.
[17] Clinicaltrials.gov. **2019**.
[18] J. Li, C. Qi, F. Zhang, Z. Li, W. Zhu, Z. Yu, K. Xiao, L. Lu, S. Mei, D. Qian, C. He, T. Ye, M. Xu, W. Yao, WO119266. **2018**.
[19] G. Sun, D. Rong, Z. Li, G. Sun, F. Wu, X. Li, H. Cao, Y. Cheng, W. Tang, Y. Sun, *Front. Cell. Dev. Biol.* **2021**, *9*, 694363.
[20] M. Giustiniano, S. Daniele, S. Pelliccia, V. La Pietra, D. Pietrobono, D. Brancaccio, S. Cosconati, A. Messere, S. Giuntini, L. Cerofolini, M. Fragai, C. Luchinat, S. Taliani, G. La Regina, F. Da Settimo, R. Silvestri, C. Martini, E. Novellino, L. Marinelli, *J. Med. Chem.* **2017**, *60*, 8115.
[21] A. Cipriano, C. Milite, A. Feoli, M. Viviano, G. Pepe, P. Campiglia, G. Sarno, S. Picaud, S. Imaide, N. Makukhin, P. Filippakopoulos, A. Ciulli, S. Castellano, G. Sbardella, *ChemMedChem* **2022**, *17*, e202200343.
[22] C. Milite, G. Amendola, A. Nocentini, S. Bua, A. Cipriano, E. Barresi, A. Feoli, E. Novellino, F. Da Settimo, C. T. Supuran, S. Castellano, S. Cosconati, S. Taliani, *J. Enzyme Inhib. Med. Chem.* **2019**, *34*, 1697.
[23] S. Taliani, I. Pugliesi, E. Barresi, F. Simorini, S. Salerno, C. La Motta, A. M. Marini, B. Cosimelli, S. Cosconati, S. Di Maro, L. Marinelli, S. Daniele, M. L. Trincavelli, G. Greco, E. Novellino, C. Martini, F. Da Settimo, *J. Med. Chem.* **2012**, *55*, 1490.
[24] R. S. Keri, A. Hiremathad, S. Budagumpi, B. M. Nagaraja, *Chem. Biol. Drug Des.* **2015**, *86*, 19.
[25] Y. F. Li, G. F. Wang, P. L. He, W. G. Huang, F. H. Zhu, H. Y. Gao, W. Tang, Y. Luo, C. L. Feng, L. P. Shi, Y. D. Ren, W. Lu, J. P. Zuo, *J. Med. Chem.* **2006**, *49*, 4790.
[26] T. L. Mistry, L. Truong, A. K. Ghosh, M. E. Johnson, S. Mehboob, *ACS Infect. Dis.* **2017**, *3*, 54.
[27] G. A. Dziwornu, D. Coertzen, M. Leshabane, C. M. Korkor, C. K. Cloete, M. Njoroge, L. Gibhard, N. Lawrence, J. Reader, M. van der Watt, S. Wittlin, L. M. Birkholtz, K. Chibale, *J. Med. Chem.* **2021**, *64*, 5198.
[28] J. J. Nué-Martinez, D. Cisneros, M. V. Moreno-Blázquez, C. Fonseca-Berzal, J. I. Manzano, D. Kraeutler, M. A. Ungogo, M. A. Aloraini, H. Elati, A. Ibáñez-Escribano, L. Lagartera, T. Herraiz, F. Gamarro, H. P. de Koning, A. Gómez-Barrio, C. Dardonville, *J. Med. Chem.* **2023**, *66*, 13452.
[29] G. Donati, V. M. D'Amore, P. Russomanno, L. Cerofolini, J. Amato, S. Marzano, M. Salobehaj, D. Rizzo, G. Assoni, A. Carotenuto, V. La Pietra, D. Arosio, P. Seneci, M. Fragai, D. Brancaccio, F. S. Di Leva, L. Marinelli, *Comput. Struct. Biotechnol. J.* **2023**, *21*, 3355.
[30] K. M. Zak, P. Grudnik, K. Guzik, B. J. Zieba, B. Musielak, A. Dömling, G. Dubin, T. A. Holak, *Oncotarget* **2016**, *7*, 30323.
[31] M. Konstantinidou, T. Zarganes-Tzitzikas, K. Magiera-Mularz, T. A. Holak, A. Dömling, *Angew. Chem. Int. Ed.* **2018**, *57*, 4840.
[32] M. Waqas, S. A. Halim, A. Alsalman, A. Khan, E. Elkord, A. Al-Harrasi, *J. Biomol. Struct. Dyn.* **2023**, 1.
[33] Glide, Schrödinger, LLC, New York, NY, **2021**.
[34] K. Guzik, K. M. Zak, P. Grudnik, K. Magiera, B. Musielak, R. Törner, L. Skalniak, A. Dömling, G. Dubin, T. A. Holak, *J. Med. Chem.* **2017**, *60*, 5857.
[35] R. Kitel, I. Rodríguez, X. del Corte, J. Atmaj, M. Żarnik, E. Surmiak, D. Muszak, K. Magiera-Mularz, G. M. Popowicz, T. A. Holak, B. Musielak, *ACS Chem. Biol.* **2022**, *17*, 2655.
[36] B. Cheng, W. Wang, X. Niu, Y. Ren, T. Liu, H. Cao, S. Wang, Y. Tu, J. Chen, S. Liu, X. Yang, J. Chen, *J. Med. Chem.* **2020**, *63*, 15946.
[37] M. Qin, Q. Cao, S. Zheng, Y. Tian, H. Zhang, J. Xie, H. Xie, Y. Liu, Y. Zhao, P. Gong, *J. Med. Chem.* **2019**, *62*, 4703.
[38] L. Di, P. V. Fish, T. Mano, *Drug Discov. Today* **2012**, *17*, 486.
[39] LigPrep, Schrödinger, LLC, New York, NY, **2021**.
[40] Epik, Schrödinger, LLC, New York, NY, **2021**.
[41] ConfGen, Schrödinger, LLC, New York, NY, **2021**.
[42] S. L. Dixon, A. M. Smondyrev, S. N. Rao, *Chem. Biol. Drug Des.* **2006**, *67*, 370.
[43] V. Limongelli, L. Marinelli, S. Cosconati, H. A. Braun, B. Schmidt, E. Novellino, *ChemMedChem* **2007**, *2*, 667.
[44] E. Da Pozzo, V. La Pietra, B. Cosimelli, F. Da Settimo, C. Giacomelli, L. Marinelli, C. Martini, E. Novellino, S. Taliani, G. Greco, *ACS Chem. Neurosci.* **2014**, *5*, 390.
[45] Maestro, Schrödinger, LLC, New York, NY, **2021**.
[46] Protein Preparation Wizard, Schrödinger, LLC, New York, NY, **2021**.
[47] G. Madhavi Sastry, M. Adzhigirey, T. Day, R. Annabhimoju, W. Sherman, *J. Comput.-Aided Mol. Des.* **2013**, *27*, 221.
[48] Prime, Schrödinger, LLC, New York, NY, **2021**.
[49] M. H. M. Olsson, C. R. Søndergaard, M. Rostkowski, J. H. Jensen, *J. Chem. Theory Comput.* **2011**, *7*, 525.
[50] J. L. Banks, H. S. Beard, Y. Cao, A. E. Cho, W. Damm, R. Farid, A. K. Felts, T. A. Halgren, D. T. Mainz, J. R. Maple, R. Murphy, D. M. Philipp, M. P. Repasky, L. Y. Zhang, B. J. Berne, R. A. Friesner, E. Gallicchio, R. M. Levy, *J. Comput. Chem.* **2005**, *26*, 1752.
[51] R. A. Friesner, R. B. Murphy, M. P. Repasky, L. L. Frye, J. R. Greenwood, T. A. Halgren, P. C. Sanschagrin, D. T. Mainz, *J. Med. Chem.* **2006**, *49*, 6177.
[52] T. A. Halgren, R. B. Murphy, R. A. Friesner, H. S. Beard, L. L. Frye, W. T. Pollard, J. L. Banks, *J. Med. Chem.* **2004**, *47*, 1750.
[53] R. A. Friesner, J. L. Banks, R. B. Murphy, T. A. Halgren, J. J. Klicic, D. T. Mainz, M. P. Repasky, E. H. Knoll, M. Shelley, J. K. Perry, D. E. Shaw, P. Francis, P. S. Shenkin, *J. Med. Chem.* **2004**, *47*, 1739.
[54] J. C. Shelley, A. Cholleti, L. L. Frye, J. R. Greenwood, M. R. Timlin, M. Uchimaya, *J. Comput.-Aided Mol. Des.* **2007**, *21*, 681.
[55] MacroModel, Schrödinger, LLC, New York, NY, **2021**.
[56] E. F. Pettersen, T. D. Goddard, C. C. Huang, E. C. Meng, G. S. Couch, T. I. Croll, J. H. Morris, T. E. Ferrin, *Protein Sci.* **2021**, *30*, 70.
[57] P. Schanda, Ē. Kupče, B. Brutscher, *J. Biomol. NMR* **2005**, *33*, 199.
[58] QikProp, version 2.3; Schrödinger, Inc., New York, **2005**

SUPPORTING INFORMATION

Additional supporting information can be found online in the Supporting Information section at the end of this article.

How to cite this article: G. Donati, M. Viviano, V. M. D'Amore, A. Cipriano, I. Diakogiannaki, J. Amato, S. Tomassi, D. Brancaccio, P. Russomanno, F. S. Di Leva, D. Arosio, P. Seneci, S. Taliani, K. Magiera-Mularz, B. Musielak, L. Skalniak, T. A. Holak, S. Castellano, V. La Pietra, L. Marinelli, *Arch. Pharm.* **2024**;*357*:e2300583. https://doi.org/10.1002/ardp.202300583